Magnetic-Field Density-Functional Theory (BDFT): Lessons from the Adiabatic Connection

Sarah Reimann,*,† Alex Borgoo,*,† Erik I. Tellgren,† Andrew M. Teale,‡ and Trygve Helgaker*,†

†*Department of Chemistry, Hylleraas Centre for Quantum Molecular Sciences, University of Oslo, P.O. Box 1033, Blindern, Oslo N-0315, Norway*

‡*School of Chemistry, University of Nottingham, University Park, Nottingham NG7 2RD, UK*

E-mail: sarah.reimann@kjemi.uio.no; alex.borgoo@kjemi.uio.no; t.u.helgaker@kjemi.uio.no

Abstract

We study the effects of magnetic fields in the context of magnetic field density-functional theory (BDFT), where the energy is a functional of the electron density ρ and the magnetic field $\mathbf{B}$. We show that this approach is a worthwhile alternative to current-density functional theory (CDFT) and may provide a viable route to the study of many magnetic phenomena using density-functional theory (DFT). The relationship between BDFT and CDFT is developed and clarified within the framework of the four-way correspondence of saddle functions and their convex and concave parents in convex analysis. By decomposing the energy into its Kohn–Sham components, we demonstrate that the magnetizability is mainly determined by those energy components that are related to the density. For existing density functional approximations, this implies that, for the magnetizability, improvements of the density will be more beneficial than introducing a magnetic-field dependence in the correlation functional. However, once a

good charge density is achieved, we show that high accuracy is likely only obtainable by including magnetic-field dependence. We demonstrate that adiabatic-connection (AC) curves at different field strengths resemble one another closely provided each curve is calculated at the equilibrium geometry of that field strength. In contrast, if all AC curves are calculated at the equilibrium geometry of the field-free system, then the curves change strongly with increasing field strength due to the increasing importance of static correlation. This holds also for density functional approximations, for which we demonstrate that the main error encountered in the presence of a field is already present at zero field strength, indicating that density-functional approximations may be applied to systems in strong fields, without the need to treat additional static correlation.

1 Introduction

Magnetic fields and their effects on atoms and molecules have for many years been an active area of research in physics and chemistry. Of particular interest are molecular magnetic properties such as NMR shielding constants and magnetizabilities, which are measurable physical observables and an important application area of quantum chemistry. We also note an interest in the effects of ultra-strong magnetic fields on atoms and molecules in astrophysics.[1–3] From a theoretical point of view, the study of molecules in ultra-strong magnetic fields can give new insight, such as the recent discovery of a hitherto unknown perpendicular paramagnetic bonding mechanism.[4]

In general, for the computation of molecular magnetic properties, the performance of Kohn–Sham density-functional theory (DFT) is still not satisfactory.[5–7] For an improvement in density-functional approximations (DFAs), it is necessary to understand the effect of a magnetic field on the components of the Kohn–Sham energy—in particular, on the correlation functional. The development of such functionals is an active field of research.[7–9] In this paper, we analyse for the first time the field dependence of the Kohn–Sham energy components, using the adiabatic connection (AC).

There are two different ways of including the effects of magnetic fields in DFT. In *current-density-functional theory* (CDFT), a current dependence is introduced in the universal density functional, which then depends on the density and paramagnetic current density.[10,11] In *magnetic-field density-functional theory* (BDFT), we introduce instead a field dependence in the density functional.[12] Here, we develop CDFT and BDFT within a common framework—namely, the four-way correspondence of conjugate saddle functions and their convex and concave parents,[13] allowing us to relate and compare the CDFT and BDFT correlation functionals.

For the construction of exchange–correlation functionals, AC curves have in the past provided useful insight.[14–21] However, so far, this has been done only in the absence of magnetic fields. To examine and understand the performance of exact DFT and of DFAs in magnetic fields, we extend the studies of AC curves to include a magnetic field, within the framework of BDFT. We consider two regimes: the weak-field regime to understand and model magnetic properties better and the strong-field regime to improve our understanding of fundamental physical and chemical concepts. We begin with weak fields, computing derivatives of the energy, relevant to molecular properties, using the finite-difference method. The energy and derivatives are decomposed into their Kohn–Sham components and analysed individually. We investigate to what extent a field dependence in the density functional may improve the computation of the magnetizability (proportional to the second derivative of the energy with respect to the magnetic field strength). Finally, we consider strong magnetic fields, studying AC curves for exact DFT and DFAs under such conditions.

The remainder of the paper is organized as follows. The structure of Kohn–Sham DFT in magnetic fields is outlined in Section 2, comparing the BDFT and CDFT formalisms. In Section 3, we introduce the AC for BDFT, allowing for a detailed analysis of the correlation energy. Computational details are given in Section 4. Our results in the weak- and strong-field regimes are presented and discussed in Section 5. Finally, Section 6 gives concluding remarks and directions for future work.

2 DFT in a magnetic field

In this section, we discuss DFT in the presence of a magnetic field—in particular, we develop CDFT and BDFT within the framework of convex conjugation, setting up and relating the Hohenberg–Kohn and Lieb variation principles for these theories. We begin with a review of DFT.

2.1 Ground-state energy in the absence of a magnetic field

In the absence of a magnetic field, the electronic Hamiltonian of an N-electron system in an external scalar potential v is given by

$$H_\lambda(v) = T + \lambda W + \sum_{i=1}^{N} v(\mathbf{r}_i), \tag{1}$$

where T is the N-electron kinetic-energy operator and W the N-electron two-electron repulsion operator. We have included in the Hamiltonian the interaction-strength parameter λ, which is equal to one for the fully interacting (physical) system and zero for the noninteracting system. According to the Rayleigh–Ritz variation principle, the ground-state energy is given by

$$E_\lambda(v) = \inf_{\gamma \in \mathcal{D}_N} \operatorname{tr} \gamma H_\lambda(v), \tag{2}$$

where $\mathcal{D}_N$ is the set of all normalized N-electron density matrices with a finite kinetic energy. With $v \in \chi^* = L^{3/2}(\mathbb{R}^3) + L^\infty(\mathbb{R}^3)$, the requirement that $\gamma \in \mathcal{D}_N$ also guarantees a finite total energy with associated density $\rho \in \chi = L^3(\mathbb{R}^3) \cap L^1(\mathbb{R}^3)$.[22]

From the linearity of $H_\lambda(v)$ in v in Eq. (1) and from the Rayleigh–Ritz variation principle in Eq. (2), it follows that $E_\lambda(v)$ is concave in v. To see this, let v_1 and v_2 be two external potentials in χ^* and select $0 < \mu < 1$. From the linearity of the Hamiltonian in the potential,

we obtain $H_\lambda(\mu v_1 + (1-\mu)v_2) = \mu H_\lambda(v_1) + (1-\mu)H_\lambda(v_2)$, from which concavity follows:

$$\begin{aligned} E_\lambda(\mu v_1 + (1-\mu)v_2) &= \inf_{\gamma\in\mathcal{D}_N} \operatorname{tr}\gamma\left(\mu H_\lambda(v_1) + (1-\mu)H_\lambda(v_2)\right) \\ &\geq \inf_{\gamma\in\mathcal{D}_N} \operatorname{tr}\gamma\mu H_\lambda(v_1) + \inf_{\gamma\in\mathcal{D}_N} \operatorname{tr}\gamma(1-\mu)H_\lambda(v_2) \\ &= \mu E_\lambda(v_1) + (1-\mu)E_\lambda(v_2). \end{aligned} \tag{3}$$

An additional property of the energy that follows from the Rayleigh–Ritz variation principle is upper semi-continuity—a weak form of continuity important in convex analysis.[23] Upper semi-continuous concave functions are said to be closed concave.

2.2 DFT in the absence of a magnetic field

From the closed concavity of the ground-state energy, it follows that there exists a unique function $F_\lambda(\rho)$, the universal density functional, such that[22]

$$E_\lambda(v) = \inf_{\rho\in\chi}\left[F_\lambda(\rho) + (v|\rho)\right], \tag{4}$$

$$F_\lambda(\rho) = \sup_{v\in\chi^*}\left[E_\lambda(v) - (v|\rho)\right], \tag{5}$$

where $(v|\rho) = \int v(\mathbf{r})\rho(\mathbf{r})\mathrm{d}\mathbf{r}$. Moreover, F is closed convex, meaning that $-F$ is closed concave. It is a general result of convex analysis that there exists a unique one-to-one correspondence between all closed convex functions on χ and all closed concave functions on its dual χ^*; see Ref. 23. The functions E_λ and F_λ, related in the manner of Eqs. (4) and (5), are said to be conjugate functions: each function contains all information needed to generate the other function by convex or concave conjugation. In the following, we will use the theory of convex conjugation to develop and relate BDFT and CDFT, within a common framework.

We refer to Eqs. (4) and (5) as the Hohenberg–Kohn and Lieb variation principles, respectively. We note that the density functional of Eq. (5) may be written in the constrained-

search form[22,24]

$$F_\lambda(\rho) = \min_{\gamma \mapsto \rho} \operatorname{tr} \gamma(T + \lambda W), \tag{6}$$

where a minimizing density always exists.

2.3 Ground-state energy in a magnetic field

Consider now an electronic system in the presence of a magnetic field $\mathbf{B}$, represented by a vector potential $\mathbf{A}$ such that $\mathbf{B} = \nabla \times \mathbf{A}$. The electronic Hamiltonian now becomes

$$H_\lambda(v, \mathbf{A}) = T(\mathbf{A}) + \lambda W + \sum_{i=1}^{N} v(\mathbf{r}_i), \tag{7}$$

where the (mechanical) kinetic-energy operator takes the form

$$T(\mathbf{A}) = \frac{1}{2} \sum_{i=1}^{N} \big(-\mathrm{i}\boldsymbol{\nabla}_i + \mathbf{A}(\mathbf{r}_i) \big)^2. \tag{8}$$

We are interested in the ground-state energy $E_\lambda(v, \mathbf{B}) = \inf_{\gamma \in \mathcal{D}_N} \operatorname{tr} \gamma H_\lambda(v, \mathbf{A})$, where the Hamiltonian is linear in v but quadratic in $\mathbf{A}$,

$$H_\lambda(v, \mathbf{A}) = H_\lambda(v) - \mathrm{i} \sum_{i=1}^{N} \mathbf{A}(\mathbf{r}_i) \cdot \nabla_i + \frac{1}{2} \sum_{i=1}^{N} A^2(\mathbf{r}_i), \tag{9}$$

where $A = |\mathbf{A}|$. As a result, $E_\lambda(v, \mathbf{B})$ is not concave in $\mathbf{B}$ and we cannot directly apply the theory of convex conjugation to the energy expressed in this manner.

To prepare for DFT, we therefore change variables from $(v, \mathbf{A})$ to $(u, \mathbf{A})$ where $u = v + \frac{1}{2}A^2$ and introduce a Hamiltonian $\bar{H}_\lambda(u, \mathbf{A})$ that is linear in both potentials[25]

$$\bar{H}_\lambda(u, \mathbf{A}) = H_\lambda(u) - \mathrm{i} \sum_{i=1}^{N} \mathbf{A}(\mathbf{r}_i) \cdot \boldsymbol{\nabla}_i. \tag{10}$$

From the Rayleigh–Ritz variation principle and the linearity of this Hamiltonian in the

potentials, it follows that the resulting ground-state energy

$$\mathcal{E}_\lambda(u, \mathbf{A}) = \inf_{\gamma \in \mathcal{D}_N} \operatorname{tr} \gamma \bar{H}_\lambda(u, \mathbf{A}) \tag{11}$$

is closed concave—both separately with respect to each variable or jointly with respect to both variables. As such, $\mathcal{E}_\lambda$ is amenable to convex conjugation, as described in the next section. The ability to apply convex analysis to $\mathcal{E}_\lambda(u, \mathbf{A})$ allows us to establish useful formal properties and relations between BDFT and CDFT. The energy may always be re-expressed in terms of v and $\mathbf{B}$ via the simple relation $E_\lambda(v, \mathbf{B}) = \mathcal{E}_\lambda(v - \frac{1}{2}A^2, \mathbf{A})$.

2.4 DFT in a magnetic field

Applying the biconjugation theorem to $\mathcal{E}_\lambda(u, \mathbf{A})$ for a fixed $\mathbf{A}$, transforming only u, we obtain the Hohenberg–Kohn and Lieb variation principles of *magnetic-field density-functional theory (BDFT)*[12]

$$\mathcal{E}_\lambda(u, \mathbf{A}) = \inf_\rho \left[\mathcal{F}_\lambda(\rho, \mathbf{A}) + (u|\rho)\right], \tag{12}$$

$$\mathcal{F}_\lambda(\rho, \mathbf{A}) = \sup_u \left[\mathcal{E}_\lambda(u, \mathbf{A}) - (u|\rho)\right], \tag{13}$$

where the density functional $\mathcal{F}_\lambda(\rho, \mathbf{A})$ is a convex–concave saddle function, closed convex in ρ for fixed $\mathbf{A}$ and concave in $\mathbf{A}$ for fixed ρ.[26] Alternatively, transforming both variables of $\mathcal{E}_\lambda(u, \mathbf{A})$, we arrive at *current-density-functional theory (CDFT)*[10,11]

$$\mathcal{E}_\lambda(u, \mathbf{A}) = \inf_{\rho, \mathbf{j}_\mathrm{p}} \left[\mathcal{G}_\lambda(\rho, \mathbf{j}_\mathrm{p}) + (u|\rho) + (\mathbf{A}|\mathbf{j}_\mathrm{p})\right], \tag{14}$$

$$\mathcal{G}_\lambda(\rho, \mathbf{j}_\mathrm{p}) = \sup_{u, \mathbf{A}} \left[\mathcal{E}_\lambda(u, \mathbf{A}) - (u|\rho) - (\mathbf{A}|\mathbf{j}_\mathrm{p})\right], \tag{15}$$

where $\mathbf{j}_\mathrm{p}$ is the paramagnetic current density and we have introduced the notation $(\mathbf{A}|\mathbf{j}_\mathrm{p}) = \int \mathbf{A}(\mathbf{r}) \cdot \mathbf{j}_\mathrm{p}(\mathbf{r}) \mathrm{d}\mathbf{r}$. The density functional $\mathcal{G}_\lambda(\rho, \mathbf{j}_\mathrm{p})$ is closed convex by construction. The

relationships between the ground-state energy $\mathcal{E}_\lambda(v, \mathbf{A})$ and the density functionals $\mathcal{F}_\lambda(\rho, \mathbf{A})$ and $\mathcal{G}_\lambda(\rho, \mathbf{j}_\mathrm{p})$ is depicted in Fig. 1, which also contains the concave–convex saddle function $\mathcal{H}_\lambda(v, \mathbf{j}_\mathrm{p})$. For the general theory of the *four-way correspondence* of Fig. 1, see Refs. 13 and 26.

From the four-way correspondence of saddle functions, it follows that BDFT and CDFT density functionals are related in the manner

$$\mathcal{F}_\lambda(\rho, \mathbf{A}) = \inf_{\mathbf{j}_\mathrm{p}} \left[\mathcal{G}_\lambda(\rho, \mathbf{j}_\mathrm{p}) + (\mathbf{A}|\mathbf{j}_\mathrm{p})\right], \tag{16}$$

$$\mathcal{G}_\lambda(\rho, \mathbf{j}_\mathrm{p}) = \sup_{\mathbf{A}} \left[\mathcal{F}_\lambda(\rho, \mathbf{A}) - (\mathbf{A}|\mathbf{j}_\mathrm{p})\right]. \tag{17}$$

Whereas Eq. (17) follows easily by substituting Eq. (13) into Eq. (15), the variation principle in Eq. (16) is more difficult to establish but follows from the general theory of saddle functions. We also note that the BDFT and CDFT density functionals may be expressed in the equivalent constrained-search form

$$\mathcal{F}_\lambda(\rho, \mathbf{A}) = \min_{\gamma \mapsto \rho} \mathrm{tr}\, \gamma \left[T(\mathbf{A}) + \lambda W\right] - \tfrac{1}{2}(A^2|\rho), \tag{18}$$

$$\mathcal{G}_\lambda(\rho, \mathbf{j}_\mathrm{p}) = \inf_{\gamma \mapsto (\rho, \mathbf{j}_\mathrm{p})} \mathrm{tr}\, \gamma (T(\mathbf{0}) + \lambda W). \tag{19}$$

Unlike for DFT in Eq. (6) and BDFT in Eq. (18), it is unknown whether a minimizing density matrix always exists in Eq. (19).

Whereas CDFT was developed by Vignale and Rasolt in 1987[10,11] and formulated in terms of convex conjugation by Tellgren *et al.* in 2012,[25] the theory of BDFT was presented by Grayce and Harris in 1994.[12] In their paper, Grayce and Harris presented two formulations of BDFT, using real or complex orbitals. We discuss here only the more conventional, complex formulation of BDFT, relating it to CDFT by the variation principles in Eqs. (18) and (19).

We note that BDFT and CDFT are considerably less developed than DFT, both formally and practically, although significant recent progress has been made in developing practical

implementations of CDFT.[7–9,27] CDFT Kohn–Sham theory may be set up in the usual manner (see Ref. 25 for further discussion). However, although the noninteracting N-representability problem has been solved for four or more Kohn–Sham orbitals in CDFT, it remains severe for single-orbital systems and an open question for two- and three-orbital systems.[28] When fractionally occupied Kohn–Sham orbitals are allowed, the CDFT N-representability problem is completely solved.[29] It is an open question whether the density functional of BDFT is easier or more difficult to model than the density functional of CDFT.

2.5 Kohn–Sham decomposition in BDFT and CDFT

Kohn–Sham theory conventionally employs a noninteracting system with integer occupation numbers, corresponding to a Slater determinant. Less commonly, fractional occupation may be considered in ensemble formalisms and occurs at the Fermi level for degenerate ground states. The Kohn–Sham decompositions of the BDFT and CDFT density functionals, respectively, are given by

$$\mathcal{F}_\lambda(\rho,\mathbf{A}) = \mathcal{T}_\mathrm{s}(\rho,\mathbf{A}) + \lambda J(\rho) + \mathcal{F}_{\mathrm{xc},\lambda}(\rho,\mathbf{A}), \tag{20}$$

$$\mathcal{G}_\lambda(\rho,\mathbf{j}_\mathrm{p}) = \mathcal{K}_\mathrm{s}(\rho,\mathbf{j}_\mathrm{p}) + \lambda J(\rho) + \mathcal{G}_{\mathrm{xc},\lambda}(\rho,\mathbf{j}_\mathrm{p}), \tag{21}$$

where $\mathcal{T}_\mathrm{s}$ and $\mathcal{K}_\mathrm{s}$ are the noninteracting ensemble BDFT and CDFT density functionals. With fractional occupation allowed, $\mathcal{T}_\mathrm{s} = \mathcal{F}_0$ and $\mathcal{K}_\mathrm{s} = \mathcal{G}_0$. In the case of integer occupations, $\mathcal{T}_\mathrm{s} \geq \mathcal{F}_0$ and $\mathcal{K}_\mathrm{s} \geq \mathcal{G}_0$, with equality for typical, nondegenerate systems. The functional $J(\rho)$ in Eqs. (20) and (21) is the Hartree functional,

$$J(\rho) = \iint \rho(\mathbf{r}_1)\rho(\mathbf{r}_2) r_{12}^{-1} \mathrm{d}\mathbf{r}_1 \mathrm{d}\mathbf{r}_2, \tag{22}$$

whereas $\mathcal{F}_{\mathrm{xc},\lambda}(\rho,\mathbf{A})$ and $\mathcal{G}_{\mathrm{xc},\lambda}(\rho,\mathbf{j}_\mathrm{p})$ are the BDFT and CDFT exchange–correlation energies, respectively. Expressing the ground-state energy $\mathcal{E}_\lambda(u,\mathbf{A})$ in terms of $\mathcal{F}_\lambda(\rho,\mathbf{A})$ and $\mathcal{G}_\lambda(\rho,\mathbf{j}_\mathrm{p})$,

we obtain

$$\begin{aligned}\mathcal{E}_\lambda(u,\mathbf{A}) &= \mathcal{T}_\mathrm{s}(\rho,\mathbf{A}) + \lambda J(\rho) + \mathcal{F}_{\mathrm{xc},\lambda}(\rho,\mathbf{A}) + (u|\rho),\\ &= \mathcal{K}_\mathrm{s}(\rho,\mathbf{j}_\mathrm{p}) + \lambda J(\rho) + \mathcal{G}_{\mathrm{xc},\lambda}(\rho,\mathbf{j}_\mathrm{p}) + (u|\rho) + (\mathbf{j}_\mathrm{p}|\mathbf{A}),\end{aligned} \tag{23}$$

where $(\rho,\mathbf{j}_\mathrm{p})$ are the minimizing ground-state density and paramagnetic current density associated with $(u,\mathbf{A})$.

From Eqs. (18) and (19), we find that the noninteracting density functionals may be expressed in the constrained-search form

$$\mathcal{T}_\mathrm{s}(\rho,\mathbf{A}) = \inf_{\gamma\mapsto\rho} \mathrm{tr}\,\gamma\, T(\mathbf{A}) - \tfrac{1}{2}(A^2|\rho), \tag{24}$$

$$\mathcal{K}_\mathrm{s}(\rho,\mathbf{j}_\mathrm{p}) = \inf_{\gamma\mapsto(\rho,\mathbf{j}_\mathrm{p})} \mathrm{tr}\,\gamma\, T(\mathbf{0}) = \inf_{\gamma\mapsto(\rho,\mathbf{j}_\mathrm{p})} \mathrm{tr}\,\gamma\, T(\mathbf{A}) - (\mathbf{A}|\mathbf{j}_\mathrm{p}) - \tfrac{1}{2}(A^2|\rho), \tag{25}$$

which upon substitution in Eq. (23) shows that the sum of the noninteracting kinetic energy and the exchange–correlation energies in BDFT and CDFT are identical:

$$\inf_{\gamma\mapsto\rho} \mathrm{tr}\,\gamma\, T(\mathbf{A}) + \mathcal{F}_\mathrm{xc}(\rho,\mathbf{A}) = \inf_{\gamma\mapsto(\rho,\mathbf{j}_\mathrm{p})} \mathrm{tr}\,\gamma\, T(\mathbf{A}) + \mathcal{G}_\mathrm{xc}(\rho,\mathbf{j}_\mathrm{p}). \tag{26}$$

Whereas the minimizing noninteracting density matrix in CDFT reproduces both the density ρ and the paramagnetic current density $\mathbf{j}_\mathrm{p}$ of the physical system, the corresponding density matrix in BDFT is required only to reproduce the density ρ. As a result, the noninteracting mechanical kinetic energy in CDFT is an upper bound to the corresponding kinetic energy in BDFT,

$$\inf_{\gamma\mapsto(\rho,\mathbf{j}_\mathrm{p})} \mathrm{tr}\,\gamma\, T(\mathbf{A}) \geq \inf_{\gamma\mapsto\rho} \mathrm{tr}\,\gamma\, T(\mathbf{A}). \tag{27}$$

From Eq. (26), it then follows that the BDFT exchange–correlation energy is an upper bound

to the corresponding CDFT exchange–correlation energy

$$\mathcal{F}_{\mathrm{xc},\lambda}(\rho,\mathbf{A}) \geq \mathcal{G}_{\mathrm{xc},\lambda}(\rho,\mathbf{j}_{\mathrm{p}}), \tag{28}$$

where $(\rho,\mathbf{j}_{\mathrm{p}})$ are the ground-state density and paramagnetic current density associated with $(u,\mathbf{A})$.

Since in BDFT the noninteracting density matrix γ of Eq. (24) needs only reproduce the density ρ (as in standard DFT), Kohn–Sham BDFT does not suffer from the N-representability problem of Kohn–Sham CDFT, where the noninteracting density matrix γ of Eq. (25) must also reproduce the paramagnetic current density $\mathbf{j}_{\mathrm{p}}$.

2.6 Density-only exchange–correlation functionals

The exact ground-state energy may be obtained from either the BDFT or CDFT variation principle, in the following alternative manners:

$$\begin{aligned}\mathcal{E}_\lambda(u,\mathbf{A}) &= \inf_{\rho}\left(\mathcal{T}_{\mathrm{s}}(\rho,\mathbf{A}) + \lambda J(\rho) + \mathcal{F}_{\mathrm{xc},\lambda}(\rho,\mathbf{A}) + (u|\rho)\right)\\ &= \inf_{\rho,\mathbf{j}_{\mathrm{P}}}\left(\mathcal{K}_{\mathrm{s}}(\rho,\mathbf{j}_{\mathrm{p}}) + \lambda J(\rho) + \mathcal{G}_{\mathrm{xc},\lambda}(\rho,\mathbf{j}_{\mathrm{p}}) + (u|\rho) + (\mathbf{j}_{\mathrm{p}}|\mathbf{A})\right).\end{aligned} \tag{29}$$

Let us now approximate the exchange–correlation functionals $\mathcal{F}_{\mathrm{xc},\lambda}(\rho,\mathbf{A})$ and $\mathcal{G}_{\mathrm{xc},\lambda}(\rho,\mathbf{j}_{\mathrm{p}})$ with the same density-only functional $F_{\mathrm{xc},\lambda}(\rho)$ in Eq. (29). We then obtain the following approximate BDFT and CDFT ground state energies, denoted by bDFT and cDFT,

$$\mathcal{E}_\lambda^{\mathrm{bDFT}}(u,\mathbf{A}) = \inf_{\rho}\left(\mathcal{T}_{\mathrm{s}}(\rho,\mathbf{A}) + \lambda J(\rho) + F_{\mathrm{xc},\lambda}(\rho) + (u|\rho)\right), \tag{30}$$

$$\mathcal{E}_\lambda^{\mathrm{cDFT}}(u,\mathbf{A}) = \inf_{\rho}\left(\inf_{\mathbf{j}_{\mathrm{P}}}\left(\mathcal{K}_{\mathrm{s}}(\rho,\mathbf{j}_{\mathrm{p}}) + (\mathbf{j}_{\mathrm{p}}|\mathbf{A})\right) + \lambda J(\rho) + F_{\mathrm{xc},\lambda}(\rho) + (u|\rho)\right). \tag{31}$$

These approximate ground-state energy functionals turn out to be identical. From the expressions for $\mathcal{T}_{\mathrm{s}}(\rho,\mathbf{A})$ and $\mathcal{K}_{\mathrm{s}}(\rho,\mathbf{j}_{\mathrm{p}})$ given in Eqs. (24) and (25), respectively, we find $\mathcal{T}_{\mathrm{s}}(\rho,\mathbf{A}) = \inf_{\mathbf{j}_{\mathrm{p}}}\left(\mathcal{K}_{\mathrm{s}}(\rho,\mathbf{j}_{\mathrm{p}}) + (\mathbf{j}_{\mathrm{p}}|\mathbf{A})\right)$ and the identification of the functionals follows. Hence,

under the approximation $\mathcal{F}_{\mathrm{xc},\lambda}(\rho,\mathbf{A}) = \mathcal{G}_{\mathrm{xc},\lambda}(\rho,\mathbf{j}_\mathrm{p}) = F_{\mathrm{xc},\lambda}(\rho)$, the BDFT and CDFT Kohn–Sham systems coincide, although the kinetic-energy functionals $\mathcal{T}_\mathrm{s}$ and $\mathcal{K}_\mathrm{s}$ remain different. As we shall see, the noninteracting kinetic energy provides the dominant magnetic contribution to the total energy, the exchange–correlation contribution being much smaller.

3 Adiabatic connection

To study of the AC in BDFT, we generalize the procedure of Teale, Coriani, and Helgaker[21] to nonzero field strengths. In this manner, high-accuracy AC curves may be generated from accurate wave functions, as will be discussed in Section 3.1. The resulting AC curves give valuable information about the role of dynamical and static correlation in BDFT. They may also be used to benchmark DFAs, whose AC curves are obtained by scaling, as discussed in Section 3.2

3.1 Adiabatic connection for BDFT

We have formulated BDFT with magnetic field $\mathbf{B}$ in terms of the gauge-dependent vector potential $\mathbf{A}$ satisfying $\mathbf{B} = \nabla \times \mathbf{A}$. To connect with the original BDFT formulation by Grayce and Harris,[12] we may rely on gauge invariance to write

$$E_\lambda(v,\mathbf{B}) = \mathcal{E}_\lambda(v - \frac{1}{2}A^2, \mathbf{A}), \tag{32}$$

$$F_\lambda(\rho,\mathbf{B}) = \mathcal{F}_\lambda(\rho,\mathbf{A}) + \frac{1}{2}(\rho|A^2), \tag{33}$$

$$T_\mathrm{s}(\rho,\mathbf{B}) = \mathcal{T}_\mathrm{s}(\rho,\mathbf{A}) + \frac{1}{2}(\rho|A^2). \tag{34}$$

Note that $\mathcal{E}_\lambda$ is a functional of u, while E_λ is a functional of v. These definitions yield the following BDFT Hohenberg–Kohn and Lieb variation principles, respectively

$$E_\lambda(v, \mathbf{B}) = \inf_\rho \left[F_\lambda(\rho, \mathbf{B}) + (v|\rho)\right], \tag{35}$$

$$F_\lambda(\rho, \mathbf{B}) = \sup_v \left[E_\lambda(v, \mathbf{B}) - (v|\rho)\right]. \tag{36}$$

In this formulation of BDFT, all quantities are manifestly gauge invariant.

To set up the AC of BDFT, we proceed in the usual manner, rewriting the density functional as

$$F_\lambda(\rho, \mathbf{B}) = T_\mathrm{s}(\rho, \mathbf{B}) + \int_0^\lambda \frac{\mathrm{d}F_\mu(\rho, \mathbf{B})}{\mathrm{d}\mu}\, \mathrm{d}\mu. \tag{37}$$

This expression is rigorous in the ensemble case, when $T_\mathrm{s}(\rho, \mathbf{B}) = F_0(\rho, \mathbf{B})$, and relies on an approximation or additional nondegeneracy assumption in the case of integer occupation. Assuming that a maximizing potential v exists in the Lieb variation principle of Eq. (34), we obtain

$$F_\lambda(\rho, \mathbf{B}) = \mathrm{tr}\, \gamma_\lambda^{\rho,\mathbf{B}} H_\lambda(0, \mathbf{B}) \tag{38}$$

where $\gamma_\lambda^{\rho,\mathbf{B}}$ is the ground-state density matrix for the maximizing potential. By the Hellmann–Feynman theorem, we then obtain the following expression for the BDFT density functional

$$F_\lambda(\rho, \mathbf{B}) = T_\mathrm{s}(\rho, \mathbf{B}) + \int_0^\lambda \mathrm{tr}\, \gamma_\mu^{\rho,\mathbf{B}}\, W\, \mathrm{d}\mu. \tag{39}$$

Introducing the BDFT exchange and correlation functionals by

$$E_\mathrm{x}(\rho, \mathbf{B}) = \mathrm{tr}\, \gamma_0^{\rho,\mathbf{B}}\, W - J(\rho), \tag{40}$$

$$E_{\mathrm{c},\lambda}(\rho, \mathbf{B}) = \int_0^\lambda \mathcal{W}_\mu(\rho, \mathbf{B})\, \mathrm{d}\mu \tag{41}$$

in terms of the field-dependent AC correlation integrand

$$\mathcal{W}_{\mathrm{c},\lambda}(\rho,\mathbf{B}) = \mathrm{tr}\left(\gamma_{\lambda}^{\rho,\mathbf{B}} - \gamma_{0}^{\rho,\mathbf{B}}\right) W, \tag{42}$$

we arrive at the BDFT density functional

$$F_{\lambda}(\rho,\mathbf{B}) = T_{\mathrm{s}}(\rho,\mathbf{B}) + \lambda J(\rho) + E_{\mathrm{xc},\lambda}(\rho,\mathbf{B}) \tag{43}$$

where $E_{\mathrm{xc},\lambda}(\rho,\mathbf{B}) = \lambda E_{\mathrm{x}}(\rho,\mathbf{B}) + E_{\mathrm{c},\lambda}(\rho,\mathbf{B})$.

We here study the BDFT correlation energy in Eq. (41) by calculating the monotonically decreasing BDFT correlation integrand $\mathcal{W}_{\mathrm{c},\lambda}(\rho,\mathbf{B})$ for interaction strengths in the interval $[0,1]$ by means of the Lieb variation principle. The quality of the AC integrand is determined by the quality of the underlying wave-function model used for $E_{\lambda}(v,\mathbf{B})$ in the Lieb variation principle in Eq. (36).

3.2 AC curves for approximate density functionals

Given the wealth of existing approximations for $E_{\mathrm{c}}(\rho)$ in DFT, we may consider developing approximations that generalize existing forms to $E_{\mathrm{c}}(\rho,\mathbf{B}) = E_{\mathrm{c},1}(\rho,\mathbf{B})$ in BDFT; in the simplest approximation, we may ignore the field dependence of $E_{\mathrm{c}}(\rho,\mathbf{B})$ entirely. To compare and evaluate such approximate functionals against the benchmark AC data, uniform scaling relations may be employed.

For an explicit approximate functional, AC curves can be computed using the formula[30]

$$\mathcal{W}_{\mathrm{c},\lambda}(\rho,\mathbf{B}) = \frac{\partial}{\partial\lambda}(\lambda^2 E_{\mathrm{c}}(\rho_{1/\lambda},\mathbf{B})), \tag{44}$$

where

$$\rho_{1/\lambda}(\mathbf{r}) = \lambda^{-3}\rho(\mathbf{r}/\lambda) = \lambda^{-3}\rho(\mathbf{r}'), \tag{45}$$

in terms of the scaled coordinate by $\mathbf{r}' = \mathbf{r}/\lambda$. The scaling formula for the BDFT correlation energy given in Eq. (44) follows in the same way as for standard DFT:

$$\begin{aligned}\mathcal{W}_{\mathrm{c},\lambda}(\rho,\mathbf{B}) &= \frac{\partial}{\partial\lambda}E_{\mathrm{c},\lambda}(\rho,\mathbf{B}) = \frac{\partial}{\partial\lambda}\left(F_\lambda(\rho,\mathbf{B}) - T_\mathrm{s}(\rho,\mathbf{B}) - \lambda J(\rho) - \lambda E_\mathrm{x}(\rho)\right)\\ &= \frac{\partial}{\partial\lambda}\lambda^2\left(F(\rho_{1/\lambda},\mathbf{B}) - T_\mathrm{s}(\rho_{1/\lambda},\mathbf{B}) - J(\rho_{1/\lambda}) - E_\mathrm{x}(\rho_{1/\lambda})\right)\\ &= \frac{\partial}{\partial\lambda}\lambda^2 E_\mathrm{c}(\rho_{1/\lambda},\mathbf{B}),\end{aligned} \tag{46}$$

where we have used Eq. (41) in the first step, Eq. (43) in the second step, the coordinate scaling relations

$$F_\lambda(\rho,\mathbf{B}) = \lambda^2 F_\lambda(\rho_{1/\lambda},\mathbf{B}), \quad T_\mathrm{s}(\rho,\mathbf{B}) = \lambda^2 T_\mathrm{s}(\rho_{1/\lambda},\mathbf{B}), \tag{47}$$

$$J(\rho) = \lambda J(\rho_{1/\lambda}), \qquad E_\mathrm{x}(\rho) = \lambda E_\mathrm{x}(\rho_{1/\lambda}), \tag{48}$$

in the third step, and finally Eq. (43) again in the last step. For a field-dependent correlation functional that depends locally on the density, the correlation energy can be obtained as

$$E_\mathrm{c}(\rho_{1/\lambda},\mathbf{B}) = \int\epsilon_\mathrm{c}(\rho_{1/\lambda}(\mathbf{r}),\mathbf{B})\,\mathrm{d}\mathbf{r} = \lambda^3\int\epsilon_\mathrm{c}(\lambda^{-3}\rho(\mathbf{r}),\mathbf{B})\,\mathrm{d}\mathbf{r}. \tag{49}$$

For functionals that also depend locally on the gradient, we have that

$$\frac{\partial\rho_{1/\lambda}(\mathbf{r})}{\partial\mathbf{r}} = \lambda^{-3}\frac{\partial\rho(\mathbf{r}')}{\partial\mathbf{r}} = \lambda^{-3}\frac{\partial\rho(\mathbf{r}')}{\partial\mathbf{r}'}\frac{\partial\mathbf{r}'}{\partial\mathbf{r}} = \lambda^{-4}\frac{\partial\rho(\mathbf{r}')}{\partial\mathbf{r}'}. \tag{50}$$

At the LDA and GGA levels of refinement, standard functionals may be employed, neglecting the field dependence.

For meta-GGA functionals, the kinetic-energy density is also needed. From Eq. (45), it

follows that the orbitals and their derivatives scale as

$$\phi_i^{1/\lambda}(\mathbf{r}) = \lambda^{-3/2}\phi_i(\mathbf{r}'), \tag{51}$$

$$\frac{\partial\phi_i^{1/\lambda}(\mathbf{r})}{\partial\mathbf{r}} = \lambda^{-\frac{3}{2}}\frac{\partial\mathbf{r}'}{\partial\mathbf{r}}\frac{\partial\phi(\mathbf{r}')}{\partial\mathbf{r}'} = \lambda^{-\frac{5}{2}}\frac{\partial\phi(\mathbf{r}')}{\partial\mathbf{r}'}, \tag{52}$$

implying that the kinetic-energy density τ_0 transforms as

$$\tau_0^{1/\lambda}(\mathbf{r}) = \frac{1}{2}\sum_{i=0}^{\text{occ}}\left|\frac{\partial\phi_i^{1/\lambda}(\mathbf{r})}{\partial\mathbf{r}}\right|^2 = \lambda^{-5}\tau_0(\mathbf{r}'). \tag{53}$$

In a magnetic field, the kinetic-energy density must be modified to ensure gauge invariance. One such modification is to use the physical kinetic-energy density proposed by Maximoff and Scuseria,[31] here given in the scaled form

$$\tau_{\text{phys}}^{1/\lambda}(\mathbf{r}) = \frac{1}{2}\sum_{l}\left|(-\mathrm{i}\nabla + \mathbf{A}(\mathbf{r}))\phi_l^{1/\lambda}(\mathbf{r})\right|^2. \tag{54}$$

Finally, from $\mathbf{A}^{1/\lambda}(\mathbf{r}) = \lambda^{-1}\mathbf{A}(\mathbf{r}')$, we obtain $\tau_{\text{phys}}^{1/\lambda}(\mathbf{r}) = \lambda^{-5}\tau_{\text{phys}}(\mathbf{r}')$. The AC curves for meta-GGAs can then be obtained by using the scaled density in Eq. (49) along with the scaled gradient in Eq. (50) and the scaled kinetic-energy density in Eq. (53), replacing τ_0 by τ_{phys}.

4 Computational details

Except where noted, all calculations have been performed using the `LONDON` quantum-chemistry software.[32,33] For evaluation of the exchange–correlation functionals, this code uses the XCFun library.[34] To ensure gauge-origin independence, London atomic orbitals[35] are used throughout. Unless otherwise stated, we use the aug-cc-pVTZ basis set of Dunning and coworkers[36,37] in Cartesian rather than spherical-harmonic form. This basis is used for both the orbital and potential expansions in the Lieb optimizations. In particular, we take the FCI or coupled-

cluster density of the interacting system ρ and perform the Lieb optimization as in Refs. 38,39, with a singular-value decomposition of 10^{-6} a.u. for the Hessian. From the one-electron density matrix generated in the Lieb optimization at $\lambda = 0$, the Kohn–Sham components $T_{\mathrm{s}}(\rho)$, $J(\rho)$, $(v|\rho)$, and $E_{\mathrm{x}}(\rho)$ are obtained directly, whereas $E_{\mathrm{c}}(\rho)$ is obtained by subtracting $T_{\mathrm{s}}(\rho) + J(\rho) + (v|\rho) + E_{\mathrm{x}}(\rho)$ from the corresponding FCI or coupled-cluster ground-state energy at $\lambda = 1$.

We have used bond lengths $1.4a_0$ for H_2, $5.7a_0$ for He_2, and $3.028a_0$ for LiH. The geometries for HF, H_2O, NH_3, CH_4, CO, and N_2 are from Refs. 5,6, optimized at the CCSD(T)/cc-pVTZ level of theory.

We remark that in all the Lieb optimizations corresponding to Eqs. (37), (38), and (39), we let the reference density $\rho = \rho(\mathbf{B})$ depend on the external magnetic field, in order to track the field-dependent ground state. Hence, the $\mathbf{B}$-dependence we see in our AC curves is a direct dependence combined with an indirect dependence due to the changing reference density.

5 Results and discussion

This section consists of two parts. First, in Section 5.1, we explore the weak-field regime by studying the magnetizability for a number of atomic and molecular systems. In Section 5.2, we study the AC at different field strengths for H_2 and LiH, yielding insight into the magnetic-field dependence of the correlation energy up to a field strength of one atomic unit, $B_0 = 2.35 \times 10^5$ T. In both subsections, the performance of various DFAs is assessed by comparing with accurate Kohn–Sham values, obtained at the full-configuration-interaction (FCI) and coupled-cluster doubles (CCD) levels of theory using the Lieb variation principle.

5.1 Magnetizability

For the singlet closed-shell atomic and molecular systems considered here, the magnetizability,

$$\xi = -\left.\frac{\mathrm{d}^2 E(B)}{\mathrm{d}B^2}\right|_{B=0}, \tag{55}$$

describes the behaviour of the system in the weak-field regime: $E(B) = E(0) - \frac{1}{2}\xi B^2 + \cdots$. Before considering ξ itself, we examine in Section 5.1.1 the dependence of the total electronic energy and its Kohn–Sham components on the magnetic field. Next, we calculate ξ and its Kohn–Sham components accurately for some small systems in Section 5.1.2, comparing with standard DFAs in Section 5.1.3. We conclude by considering the importance of the field dependence of the BDFT correlation functional in Section 5.1.4.

5.1.1 Energy of H_2 in a perpendicular magnetic field

In Fig. 2, we have plotted the FCI/aug-cc-pVTZ energy of H_2 and its Kohn–Sham components against the strength of a perpendicular magnetic field, relative to the corresponding zero-field values. The plot covers a wide field range, up to $0.03B_0$ (about 7000 T). The calculated energies correspond to the points in the figure. For the total energy, the curves joining these points are plots of $E(B) - E(0) \approx -\frac{1}{2}\xi B^2$, whose curvature is $-\xi$. Similar functions are plotted for the Kohn–Sham energy components against the field strength. In Table 1, we have listed the total energy and the Kohn–Sham components at zero field and at $0.03B_0$. All calculations have been carried out at the zero-field equilibrium geometry of H_2.

The total energy of H_2 increases diamagnetically in the field, with a large positive contribution from $T_\mathrm{s}(\rho, \mathbf{B})$, a large negative contribution from $(v|\rho)$, and smaller but still large contributions from $J(\rho) > 0$ and $E_\mathrm{x}(\rho, \mathbf{B}) < 0$. The Kohn–Sham correlation energy $E_\mathrm{c}(\rho, \mathbf{B})$ makes a much smaller (negative) contribution. For this particular system, the Hartree energy $J(\rho)$ changes in a manner that closely follows that of the total energy. While the increase in $T_\mathrm{s}(\rho, \mathbf{B})$ in the field is a reflection of the induced precessional motion of the

electrons (closed-shell diamagnetism), the increase in $J(\rho)$ and the decrease in $(v|\rho)$ and $E_{\mathrm{x}}(\rho, \mathbf{B})$ follow from the concomitant contraction of the atomic densities in the field.

The quadratic curve $-\frac{1}{2}\xi B^2$ describes the field variation of the total energy (and likewise for the Kohn–Sham components) to a remarkably high accuracy over the full field range in Fig. 2.

Adding the nuclear repulsion to the total electronic energy in Table 1, we obtain $E_{\mathrm{tot}}(B = 0.0B_0) = -1.1730E_{\mathrm{h}}$ and $E_{\mathrm{tot}}(B = 0.03B_0) = -1.1726E_{\mathrm{h}}$. These FCI results at the aug-cc-pVTZ level can be compared with the parallel-field quantum-Monte-Carlo results for H_2 of Doma et al.,[40] where a quadratic fit for small field strengths up to $B = 0.05B_0$ gives $E^{\mathrm{ref}}_{\mathrm{tot}}(B = 0.03B_0) = -1.1722E_{\mathrm{h}}$, with $E^{\mathrm{ref}}_{\mathrm{tot}}(B = 0.0) = -1.1734E_{\mathrm{h}}$.

Table 1: The total electronic energy and its Kohn–Sham components of H_2 with bond distance $1.4a_0$ at zero field and at $B = 0.03B_0$ (perpendicular) calculated at the FCI/aug-cc-pVTZ level (atomic units, E_{h}).

	E	T_{s}	J	$(v\|\rho)$	E_{x}	E_{c}
$B = 0.00$	−1.8870	1.1381	1.3217	−3.6461	−0.6608	−0.0399
$B = 0.03$	−1.8867	1.1389	1.3220	−3.6468	−0.6610	−0.0398

5.1.2 FCI Kohn–Sham magnetizabilities

Table 2 contains the magnetizability ξ and its Kohn–Sham components for H_2, He, He_2, and Be calculated at the FCI/aug-cc-pVTZ level of theory and for LiH at the FCI/cc-pVTZ level for theory. For the diatomic systems, the field direction is perpendicular to the molecular axis. All derivatives have been obtained by finite difference, using the `LONDON` code for different values of the magnetic field.

The magnitudes and signs of the Kohn–Sham contributions to the magnetizability ξ in Table 2 are as expected from the discussion in Section 5.1.1. In particular, electron correlation

Table 2: The magnetizability ξ and its Kohn–Sham components calculated using FCI/aug-cc-pVTZ theory (FCI/cc-pVTZ for LiH) (atomic units, $E_\mathrm{h}B_0^{-2}$ and perpendicular field)

	ξ	ξ_{T_s}	ξ_J	ξ_v	ξ_x	ξ_c
H_2	−0.763	−1.877	−0.751	1.475	0.375	0.014
He	−0.399	−1.197	−0.434	1.019	0.217	−0.004
He_2	−0.798	−2.392	−0.874	2.043	0.434	−0.008
Be	−2.721	−8.032	−6.380	10.324	1.221	0.162
LiH	−2.010	−5.254	−5.467	6.851	1.915	−0.063

makes the smallest contribution to ξ, with ξ_c ranging from −1% for He to 6% for Be. Although fairly small, the correlation contribution to the magnetizability varies widely in magnitude and sign for the different systems, suggesting competing effects.

It is worth commenting on the magnetizability of the ^{1}S atoms He and Be. For these atoms, there is no paramagnetic contribution to ξ, which is a simple expectation value $\xi_{T_\mathrm{s}}^\mathrm{dia} = -\frac{1}{6}\int\rho(\mathbf{r})r^2\,\mathrm{d}\mathbf{r}$. In our finite-difference calculations, this term enters as part of the kinetic-energy contribution ξ_{T_s}, which also contains nonvanishing canonical kinetic-energy contribution $\xi_{T_\mathrm{s}}^\mathrm{can}$. The sum of the contributions to the magnetizability from the canonical kinetic energy and all other Kohn–Sham terms vanishes for ^{1}S atoms: $\xi_{T_\mathrm{s}}^\mathrm{can}+\xi_J+\xi_v+\xi_\mathrm{x}+\xi_\mathrm{c} = 0$.

5.1.3 DFA Kohn–Sham magnetizabilities

Table 3 contains, for the PBE, BLYP, B97, and TPSS exchange–correlation functionals, the errors in the Kohn–Sham contributions to the magnetizability of H_2 relative to the FCI/aug-cc-pVTZ contributions listed in Table 2.

The use of an approximate exchange–correlation functional affects the magnetizability of an atom or a molecule in two ways. First, it gives an error in the optimized ground-state density in the Hohenberg–Kohn variation principle; second, it gives an error in the exchange–correlation contribution to the magnetizability calculated from a given density. With this in mind, we have in Table 3 listed the errors in the Kohn–Sham components (relative to the FCI values) calculated both from the FCI ground-state density and from the ground-state density optimized using the given approximate exchange–correlation functional.

Table 3: The magnetizability ξ and its Kohn–Sham components for H_2 in a perpendicular magnetic field, calculated using FCI theory and various DFAs. For the DFA calculations the results are given both with the FCI density and the DFA density (atomic units, $E_h B_0^{-2}$). All DFA values are relative to the FCI values, irrespective of the density used in the DFA evaluation. For TPSS, we work with τ_{phys} of Eq. (54).

		ξ	ξ_{T_s}	ξ_J	ξ_v	ξ_{xc}
FCI		-0.763	-1.877	-0.751	1.475	0.390
ΔPBE	@ ρ_{FCI}	-0.036	0	0	0	-0.036
ΔBLYP	@ ρ_{FCI}	-0.033	0	0	0	-0.033
ΔB97	@ ρ_{FCI}	-0.024	0	0	0	-0.024
ΔTPSS	@ ρ_{FCI}	-0.016	0	0	0	-0.016
ΔPBE	@ ρ_{PBE}	-0.022	-0.065	-0.069	$+0.102$	$+0.010$
ΔBLYP	@ ρ_{BLYP}	-0.025	-0.071	-0.073	$+0.110$	$+0.009$
ΔB97	@ ρ_{B97}	-0.011	-0.030	-0.039	$+0.051$	$+0.007$
ΔTPSS	@ ρ_{TPSS}	-0.002	-0.015	-0.027	$+0.030$	$+0.011$

From Table 3, we see that the use of the FCI ground-state density gives an error in ξ ranging from $-0.016 E_h B_0^{-2}$ (2%) for the TPSS functional to $-0.036 E_h B_0^{-2}$ (5%) for the PBE functional. Since the FCI density is used, the errors arise only from the exchange–correlation functional, all other Kohn–Sham terms having been treated exactly. The error of the approximate exchange–correlation functionals evaluated with their own self–consistent density ranges from 5% to 10%.

For each approximate exchange-correlation functional in Table 3, the error in ξ is smallest when ξ is calculated from the optimized self-consistent field (SCF) density, with errors ranging from $-0.002 E_h B_0^{-2}$ for the TPSS functional to $-0.025 E_h B_0^{-2}$ for the BLYP functional. Among the four contributions to the total magnetizability ξ, we observe in all cases a largest (positive) error in ξ_v, with slightly smaller (but negative) errors in ξ_J and ξ_{T_s}. In all cases, the smallest error is in ξ_{xc}. It is noteworthy that the error in ξ_{xc} changes sign from negative for the FCI density to positive for the SCF density, while its magnitude is reduced by a factor of two to four. However, because of error cancellations, the error in ξ is of the same order of magnitude as the error in ξ_{xc}. Since ξ_{T_s}, ξ_J and ξ_v are determined by the density, improved magnetizabilities in

actual Kohn-Sham calculations, with a DFA, require an exchange-correlation functional that yields both superior SCF electron densities and more accurate $\xi_{\rm xc}$ values. The challenge of obtaining accurate electron densities with DFAs has very recently been highlighted in Ref. 41. In the next section, we will explore the importance of including an explicit field dependence in the correlation functional, to reduce the exchange–correlation error.

5.1.4 Field-contribution to $\xi_{\rm c}$ in BDFT

Practically all Kohn–Sham BDFT calculations of magnetizabilities use standard exchange–correlation functionals, ignoring the field dependence. Having studied the errors of typical DFAs, we now consider the importance of the field dependence of the correlation functional $E_{\rm c}(\rho, \mathbf{B})$ in BDFT. In Refs. 6 and 42, we studied in a similar manner the importance of the current contribution to the correlation functional $E_{\rm c}(\rho, \mathbf{j}_{\rm p})$ in CDFT, for NMR constants.

In Table 4, we have, for a number of systems, calculated the CCSD(T) magnetizability $\xi_{\rm CC}$ and its correlation contribution, as obtained by subtracting the Hartree–Fock magnetizability $\xi_{\rm HF}$. The CCSD(T) correlation contribution of the magnetizability $\xi_{\rm corr} = \xi_{\rm CC} - \xi_{\rm HF}$ is to a good approximation equal to the correlation contribution $\xi_{\rm c}$ in BDFT.

To estimate the field contribution to $\xi_{\rm c}$, we have calculated, by the Lieb variation principle, the Kohn–Sham potential, orbitals, and orbital energies corresponding to the CCSD(T) density. From these Kohn–Sham quantities, we have calculated the magnetizability $\xi_{\rm KS(CC)}$ by standard linear-response theory, neglecting all field dependence. Finally, the field contribution to $\xi_{\rm c}$ is estimated as $\xi_{\rm c}^{\rm B} = \xi_{\rm CC} - \xi_{\rm KS(CC)}$. For the total magnetizability, we used the `CFOUR` code;[43] for the Lieb calculation, the `DALTON` code.[44,45]

For the noble gas atoms He and Ne, there is no field contribution: $\xi_{\rm c}^{\rm B} = 0$. For the molecules studied, $\xi_{\rm c}^{\rm B}$ ranges from about 7% of the total correlation contribution for the HF molecule to 66% for CO and 154% for N_2. Clearly, *the accurate calculation of magnetizabilities*

Table 4: The CCSD(T)/aug-cc-pVQZ magnetizability ξ_{CC}, the CCSD(T) correlation contribution ξ_{corr}, and the field contribution $\xi_{\mathrm{c}}^{\mathrm{B}}$ to the BDFT correlation term ξ_{c}. In the first column, the total magnetizability is for comparison given in SI units ($\mathrm{JT}^{-2}10^{-30}$), the remaining numbers are in atomic units ($E_{\mathrm{h}}B_0^{-2}$).

	ξ_{CC} (SI)	ξ_{CC}	ξ_{corr}	$\xi_{\mathrm{c}}^{\mathrm{B}}$
He	−31.42	−0.398	−0.003	0.0
Ne	−126.0	−1.597	−0.035	0.0
HF	−176.9	−2.242	−0.055	−0.004
H_2O	−236.1	−2.992	−0.062	−0.010
NH_3	−291.2	−3.643	−0.048	−0.012
CH_4	−319.7	−4.052	−0.077	−0.045
CO	−210.9	−2.673	−0.082	−0.054
N_2	−206.2	−2.613	−0.045	−0.068

in Kohn–Sham theory is only possible with the inclusion of a field dependence in the correlation functional $E_c(\rho, \mathbf{B})$.

These results are consistent with previous work[5] and consistent with the magnitude of induced currents in these molecules—see, for example, Ref. 46 for plots of induced currents. Around the hydrogen atoms, the currents are generally weak and as such the systems with only one heavy atom and multiple hydrogen atoms (HF, H_2O, NH_3) have magnetizabilities that depend only weakly on the current corrections.

5.2 Adiabatic connection in a magnetic field

In this section, we consider the AC for molecules in a magnetic field. We begin by calculating and modelling accurate FCI AC curves of H_2 and LiH in Section 5.2.1 (at the zero-field equilibrium geometry) and in Section 5.2.2 (at the field optimized geometry). Finally, in Section 5.2.3, the performance of some standard DFAs is analysed by comparing their AC curves with the corresponding FCI curves.

5.2.1 FCI AC curves at a fixed geometry

In Fig. 3, we have plotted AC curves for H_2 at its zero-field equilibrium geometry, in a perpendicular magnetic field of different field strengths B. With increasing field strength,

the curves become more bent, indicative of increasing importance of static correlation. The explanation of this behaviour is as follows: In the magnetic field, the atomic densities contract, decreasing the overlap between the two atoms and reducing the equilibrium bond length.[4] If we now increase the field strength while maintaining the geometry at the zero-field equilibrium, the bond length will always be larger than the equilibrium at the given field strength. This effective stretching of the bond through the magnetic field is accompanied with increased static correlation.

Table 5: Field dependence of the THC parameters $s = \mathcal{W}'_{\mathrm{THC}}(0)$ and $a = \mathcal{W}_{\mathrm{THC}}(1)$, (atomic units, E_{h})

		0.0	0.2	0.4	0.6	0.8
global fit	s	−0.131	−0.134	−0.142	−0.153	−0.167
	a	−0.192	−0.195	−0.202	−0.211	−0.219
end-point fit	s	−0.125	−0.128	−0.135	−0.145	−0.157
	a	−0.208	−0.211	−0.220	−0.230	−0.241

We now apply the AC model developed by Teale, Helgaker, and Coriani (THC) in Ref. 21. The THC AC integrand is given by

$$\mathcal{W}_{\mathrm{THC}}(\lambda) = \frac{as\lambda(4a + s\lambda)}{(2a + s\lambda)^2}, \tag{56}$$

where $s = \mathcal{W}'_{\mathrm{THC}}(0)$ is the initial slope and $a = \mathcal{W}_{\mathrm{THC}}(\infty)$ is the asymptotic value in the strongly interacting limit. The parameters s and a may be fitted for $\mathcal{W}_{\mathrm{THC}}(\lambda)$ to reproduce $\mathcal{W}(\lambda)$ calculated *ab initio*. The THC model performs best when s and a are fitted globally, but a good agreement is also obtained by adjusting s and a to give $\mathcal{W}'_{\mathrm{THC}}(0) = \mathcal{W}'(0)$ and $\mathcal{W}_{\mathrm{THC}}(1) = \mathcal{W}(1)$, which is achieved by setting $s = \mathcal{W}'(0)$ and then

$$a = \frac{s^2 - 4st + s\sqrt{s^2 + 8st}}{8(t - s)} \tag{57}$$

with $t = \mathcal{W}(1)$. Although based on Görling–Levy perturbation theory, the THC model is able to capture static correlation.[21]

In Fig. 3, the globally fitted AC curve is hardly visible due to its good agreement with the exact AC curve, whereas the curve with $s = \mathcal{W}'(0)$ and $a = \mathcal{W}(1)$ deviates slightly but is still very close, capturing the correct overall behaviour—namely, the increase of static correlation with increasing field strength. The end-point fitted curve becomes only marginally worse with increasing magnetic field strength. For longer bond lengths of $3a_0$ and $5a_0$, the model performs slightly worse, but this is already true at zero field strength (see Ref. 21) and not primarily an effect of the magnetic field.

Table 5 shows how the THC parameters change with increasing magnetic field. The s parameter agrees better between the two fits than does the a parameter. The second (physically more justified) fit reveals how the initial AC slope s becomes more negative with increasing magnetic field. The slope increases in magnitude more strongly in stronger magnetic fields.

Our calculations indicate that the same models (such as the two-parameter THC model) can be used for AC curves with and without magnetic fields. However, we have not attempted here to model directly the changes in the s and a parameters induced by the field in the TCH model. Such an approach may be a useful way to add empirical field corrections to existing DFA correlation functionals.

5.2.2 FCI AC curves at optimized geometry

At a fixed geometry, the effective bond stretching leads to an increased curvature of the AC curves with increasing field strength, corresponding to an increase of static correlation. This effect is removed by calculating the AC curve at the optimized equilibrium geometry for each field strength. Indeed, Fig. 4 reveals that, when studied at the field-dependent equilibrium geometry, the AC curve is not much affected by the magnetic field.

Integrating the AC curves $\mathcal{W}(\lambda)$ from $\lambda = 0$ to $\lambda = 1$, we obtain the correlation energy.

From zero field to a field strength of $0.6B_0$, the correlation energy of H_2 changes by only $-0.002E_h$. The corresponding change in the kinetic correlation energy is about $0.002E_h$, as expected in the dynamical correlation regime, in which the kinetic correlation energy is approximately equal to minus the total correlation energy.

In Fig. 5, we have plotted the difference between AC curves in a field and the zero-field curves, normalized by the factor B^2,

$$\Delta\mathcal{W}_{c,\lambda}(B) = \frac{\mathcal{W}_{c,\lambda}(\rho_B, B) - \mathcal{W}_{c,\lambda}(\rho_0, 0)}{B^2}. \tag{58}$$

In the weak-field regime, this quantity depends on λ but is independent of B. Any variation with B in Fig. 5 is therefore an indication of higher-order effects. For H_2 and LiH, these effects are in the opposite direction to the quadratic response. There is also a reduced curvature with respect to λ with increasing field strength. At least for the systems studied, we take the pronounced trends to indicate that $\mathcal{W}_{c,\lambda}(\rho_B, B)$ can be modelled as the sum of $\mathcal{W}_{c,\lambda}(\rho_0, 0)$ and an additive correction in the strong-field regime $B \sim B_0$.

5.2.3 DFA AC curves at optimized geometry

Finally, we consider AC curves for molecules in a strong magnetic field for some standard DFAs. In Fig. 6, AC curves for H_2 and LiH at $B = 0$ and $B = 0.6B_0$ for several DFAs are compared with the corresponding FCI curve for H_2 and the CCD curve for LiH. The DFA curves have been calculated using the self-consistently optimized DFA ground-state density. Calculations on H_2 showed that use of the FCI density (in place of the self-consistent DFA density) has no visible impact on the AC curves.

The plots show that the behaviour of the AC curves is similar at the two field strengths. Among the DFAs, the TPSS functional performs best relative to FCI theory, while the LYP curve shows a considerably poorer curvature than the other DFAs.

For LiH, all DFAs yield a too steep initial slope; see Table 6. For H_2, the PBE and

TPSS(τ_{phys}) initial slopes are slightly steeper than the FCI slope, while the LYP slope is less steep, both with and without magnetic field. Since the AC curve integrates to the total correlation energy, a steeper initial slope is necessary for an increased absolute correlation energy. This behaviour is correctly captured by the PBE and TPSS(τ_{phys}) functionals but not by the LYP functional.

Table 6: For the AC curves of Fig. 6, the initial slope is given for all considered functionals (atomic units, B in B_0 and slopes in E_{h}.)

	B	Lieb	PBE	LYP	TPSS
H_2	0.0	−0.095	−0.104	−0.097	−0.101
	0.6	−0.097	−0.109	−0.090	−0.105
LiH	0.0	−0.149	−0.186	−0.265	−0.194
	0.6	−0.141	−0.206	−0.256	−0.208

6 Conclusions

The extensions of DFT to systems in the presence of magnetic fields, magnetic-field density-functional theory (BDFT) and current density-functional theory (CDFT), were introduced within the framework of convex analysis. In particular, the four-way correspondence of saddle functions and their concave and convex parents was used to elucidate the relationships between these alternative DFT approaches to molecules in a magnetic field. The Kohn–Sham decompositions of the density functionals in BDFT and CDFT were compared and a relationship between their exchange–correlation functionals was established; the BDFT exchange–correlation energy being an upper bound to the CDFT exchange–correlation energy.

The effect of a magnetic field on the Kohn–Sham energy components in BDFT was studied using high-level *ab initio* theory. In the weak-field regime, the second derivative of the energy with respect to the magnetic field (i.e., the negative magnetizability) and its contributions were studied in detail. Our calculations highlighted the fact that present DFAs give poor

charge densities, suggesting that significant improvements can only be obtained by developing DFAs with improved SCF densities. For the molecules studied, the field-dependence of the BDFT correlation energy contributes up to 2.6% of the total magnetizability (for N_2), which is comparable to the total correlation contribution. Hence, once accurate charge densities are achieved, field-dependent contributions cannot be neglected for high-accuracy calculations.

To analyse the role of electron correlation in BDFT further, we studied the AC integrand at different field strengths. At a fixed molecular geometry, a compression of the charge density with increasing field strength leads to an increased amount of static correlation (increased curvature of the AC curve). However, this effect is relatively subtle and existing models for the AC integrand are able to capture this behaviour. For the DFAs considered here, the most accurate AC integrands were provided by generalized meta-GGA functionals in the context of BDFT, consistent with previous findings for CDFT.[7] However, the dominant errors in the correlation functionals are those already present in the absence of a field, indicating the need for an improvement in the parent zero-field functionals and their associated charge densities before the benefit of field-dependent corrections can be realized.

Acknowledgements

This work was supported by the Norwegian Research Council through the CoE Grant Nos. 179568/V30 and through the European Research Council under the European Union Seventh Framework Program through the Advanced Grant ABACUS, ERC Grant Agreement No. 267683. AMT is grateful for support from a Royal Society University Research Fellowship and the Engineering and Physical Sciences Research Council EPSRC, Grant No. EP/M029131/1. EIT was supported by the Norwegian Research Council through Grant No. 240774.

References

(1) Wickramasinghe, D. T.; Ferrario, L. Magnetism in Isolated and Binary White Dwarfs. *PASP* **2000**, *112*, 873.

(2) Price, D. J.; Rosswog, S. Producing Ultrastrong Magnetic Fields in Neutron Star Mergers. *Science* **2006**, *312*, 719–722.

(3) Gourgouliatos, K. N.; Wood, T. S.; Hollerbach, R. Magnetic field evolution in magnetar crusts through three-dimensional simulations. *Proc. Nat. Acad. Sci.* **2016**, *113*, 3944–3949.

(4) Lange, K. K.; Tellgren, E. I.; Hoffmann, M. R.; Helgaker, T. A Paramagnetic Bonding Mechanism for Diatomics in Strong Magnetic Fields. *Science* **2012**, *337*, 327–331.

(5) Lutnæs, O. B.; Teale, A. M.; Helgaker, T.; Tozer, D. J.; Ruud, K.; Gauss, J. Benchmarking density-functional-theory calculations of rotational g tensors and magnetizabilities using accurate coupled-cluster calculations. *J. Chem. Phys.* **2009**, *131*, 144104.

(6) Teale, A. M.; Lutnæs, O. B.; Helgaker, T.; Tozer, D. J.; Gauss, J. Benchmarking density-functional theory calculations of NMR shielding constants and spin–rotation constants using accurate coupled-cluster calculations. *J. Chem. Phys.* **2013**, *138*.

(7) Furness, J. W.; Verbeke, J.; Tellgren, E. I.; Stopkowicz, S.; Ekström, U.; Helgaker, T.; Teale, A. M. Current Density Functional Theory Using Meta-Generalized Gradient Exchange-Correlation Functionals. *J. Chem. Theory Comput.* **2015**, *11*, 4169–4181.

(8) Zhu, W.; Zhang, L.; Trickey, S. B. Comparative studies of density-functional approximations for light atoms in strong magnetic fields. *Phys. Rev. A* **2014**, *90*, 022504.

(9) Zhu, W.; Zhang, L.; Trickey, S. B. Random phase approximation with second-order screened exchange for current-carrying atomic states. *J. Chem. Phys.* **2016**, *145*, 224106.

(10) Vignale, G.; Rasolt, M. Density-functional theory in strong magnetic fields. *Phys. Rev. Lett.* **1987**, *59*, 2360–2363.

(11) Vignale, G.; Rasolt, M. Current- and spin-density-functional theory for inhomogeneous electronic systems in strong magnetic fields. *Phys. Rev. B* **1988**, *37*, 10685–10696.

(12) Grayce, C. J.; Harris, R. A. Magnetic-field density-functional theory. *Phys. Rev. A* **1994**, *50*, 3089–3095.

(13) Rockafellar, R. T. A general correspondence between dual minimax problems and convex programs. *Pacific J. Math.* **1968**, *25*, 597–611.

(14) Becke, A. D. A new mixing of Hartree–Fock and local densityfunctional theories. *J. Chem. Phys.* **1993**, *98*, 1372–1377.

(15) Ernzerhof, M. Construction of the adiabatic connection. *Chem. Phys. Lett.* **1996**, *263*, 499 – 506.

(16) Seidl, M.; Perdew, J. P.; Kurth, S. Simulation of All-Order Density-Functional Perturbation Theory, Using the Second Order and the Strong-Correlation Limit. *Phys. Rev. Lett.* **2000**, *84*, 5070.

(17) Peach, M. J. G.; Teale, A. M.; Tozer, D. J. Modeling the adiabatic connection in H2. *J. Chem. Phys.* **2007**, *126*.

(18) Peach, M. J. G.; Miller, A. M.; Teale, A. M.; Tozer, D. J. Adiabatic connection forms in density functional theory: H2 and the He isoelectronic series. *J. Chem. Phys.* **2008**, *129*.

(19) Gori-Giorgi, P.; Vignale, G.; Seidl, M. Electronic Zero-Point Oscillations in the Strong-Interaction Limit of Density Functional Theory. *J. Chem. Theory Comput.* **2009**, *5*, 743.

(20) Kim, J.; Jung, Y. Analytical Double-Hybrid Density Functional Based on the Polynomial Series Expansion of Adiabatic Connection: A Quadratic Approximation. *J. Chem. Theory Comput.* **2015**, *11*, 45–54.

(21) Teale, A. M.; Coriani, S.; Helgaker, T. Accurate calculation and modeling of the adiabatic connection in density functional theory. *J. Chem. Phys.* **2010**, *132*, 164115.

(22) Lieb, E. H. Density functionals for coulomb systems. *Int. J. Quantum Chem.* **1983**, *24*, 243.

(23) van Tiel, J. *Convex Analysis: An Introductory Text*; Wiley, 1984.

(24) Levy, M. Universal Variational Functionals od Electron-Densities, 1st-order Density-Matrices, and Natural Spin-Orbitals and Solutions of the V-representability Problem. *Proc. Natl. Acad. Sci. U.S.A.* **1979**, *76*, 6062.

(25) Tellgren, E. I.; Kvaal, S.; Sagvolden, E.; Ekström, U.; Teale, A. M.; Helgaker, T. Choice of basic variables in current-density-functional theory. *Phys. Rev. A* **2012**, *86*, 062506.

(26) Barbu, V.; Precupano, T. *Convexity and Optimization in Banach Spaces*, 4th ed.; Springer, 2014.

(27) Tellgren, E. I.; Teale, A. M.; Furness, J. W.; Lange, K. K.; Ekström, U.; Helgaker, T. Non-perturbative calculation of molecular magnetic properties within current-density functional theory. *J. Chem. Phys.* **2014**, *140*, 034101.

(28) Lieb, E. H.; Schrader, R. Current densities in density-functional theory. *Phys. Rev. A* **2013**, *88*, 032516.

(29) Tellgren, E. I.; Kvaal, S.; Helgaker, T. Fermion N-representability for prescribed density and paramagnetic current density. *Phys. Rev. A* **2014**, *89*, 012515.

(30) Levy, M.; Perdew, J. P. Hellmann-Feynman, virial, and scaling requisites for the exact universal density functionals. Shape of the correlation potential and diamagnetic susceptibility for atoms. *Phys. Rev. A* **1985**, *32*, 2010–2021.

(31) Maximoff, S. N.; Scuseria, G. E. Nuclear magnetic resonance shielding tensors calculated with kinetic energy density-dependent exchange-correlation functionals. *Chem. Phys. Lett.* **2004**, *390*, 408–412.

(32) Tellgren, E. I.; Soncini, A.; Helgaker, T. Nonperturbative ab initio calculations in strong magnetic fields using London orbitals. *J. Chem. Phys.* **2008**, *129*, 154114.

(33) LONDON, an ab-initio program package for calculations in finite magnetic fields, founded by E. I. Tellgren, A. Soncini and T. Helgaker. Programming by E. I. Tellgren (main programmer), K. K. Lange, A. M. Teale, U. E. Ekström, S. Stopkowicz and J. H. Austad. 2016.

(34) Ekström, U.; Visscher, L.; Bast, R.; Thorvaldsen, A. J.; Ruud, K. Arbitrary-Order Density Functional Response Theory from Automatic Differentiation. *J. Chem. Theory Comput.* **2010**, *6*, 1971–1980.

(35) London, F. Théorie quantique des courants interatomiques dans les combinaisons aromatiques. *J. Phys. Radium* **1937**, *8*, 397–409.

(36) Dunning, T. H. Gaussian basis sets for use in correlated molecular calculations. I. The atoms boron through neon and hydrogen. *J. Chem. Phys.* **1989**, *90*, 1007–1023.

(37) Woon, D. E.; Dunning, T. H. Gaussian basis sets for use in correlated molecular calculations. IV. Calculation of static electrical response properties. *J. Chem. Phys.* **1994**, *100*, 2975–2988.

(38) Wu, Q.; Yang, W. A direct optimization method for calculating density functionals

and exchange-correlation potentials from electron densities. *J. Chem. Phys.* **2003**, *118*, 2498–2509.

(39) Teale, A. M.; Coriani, S.; Helgaker, T. The calculation of adiabatic-connection curves from full conguration-interaction densities: Two-electron systems. *J. Chem. Phys.* **2009**, *130*, 104111.

(40) Doma, S. B.; Abu-Shady, M.; El-Gammal, F. N.; Amer, A. A. Ground states of the hydrogen molecule and its molecular ion in the presence of a magnetic field using the variational Monte Carlo method. *Mol. Phys.* **2016**, *114*, 1787–1793.

(41) Medvedev, M. G.; Bushmarinov, I. S.; Sun, J.; Perdew, J. P.; Lyssenko, K. A. Density functional theory is straying from the path toward the exact functional. *Science* **2017**, *355*, 49–52.

(42) Reimann, S.; Ekström, U.; Stopkowicz, S.; Teale, A. M.; Borgoo, A.; Helgaker, T. The importance of current contributions to shielding constants in density-functional theory. *Phys. Chem. Chem. Phys.* **2015**, *17*, 18834–18842.

(43) CFOUR, a quantum chemical program package written by J.F. Stanton, J. Gauss, M.E. Harding, P.G. Szalay with contributions from A.A. Auer, R.J. Bartlett, U. Benedikt, C. Berger, D.E. Bernholdt, Y.J. Bomble, L. Cheng, O. Christiansen, M. Heckert, O. Heun, C. Huber, T.-C. Jagau, D. Jonsson, J. Jusélius, K. Klein, W.J. Lauderdale, D.A. Matthews, T. Metzroth, L.A. Mück, D.P. O'Neill, D.R. Price, E. Prochnow, C. Puzzarini, K. Ruud, F. Schiffmann, W. Schwalbach, C. Simmons, S. Stopkowicz, A. Tajti, J. Vázquez, F. Wang, J.D. Watts and the integral packages MOLECULE (J. Almlöf and P.R. Taylor), PROPS (P.R. Taylor), ABACUS (T. Helgaker, H.J. Aa. Jensen, P. Jørgensen, and J. Olsen), and ECP routines by A. V. Mitin and C. van Wüllen. For the current version, see http://www.cfour.de. 2016.

(44) Dalton, a molecular electronic structure program, Release Dalton2015.0 (2015), see http://daltonprogram.org. 2016.

(45) Aidas, K. et al. The Dalton quantum chemistry program system. *WIREs Comput. Mol. Sci.* **2015**, *4*, 269–284.

(46) Soncini, A.; Teale, A. M.; Helgaker, T.; Proft, F. D.; Tozer, D. J. Maps of current-density using density-functional methods. *J. Chem. Phys.* **2008**, *129*, 074101.

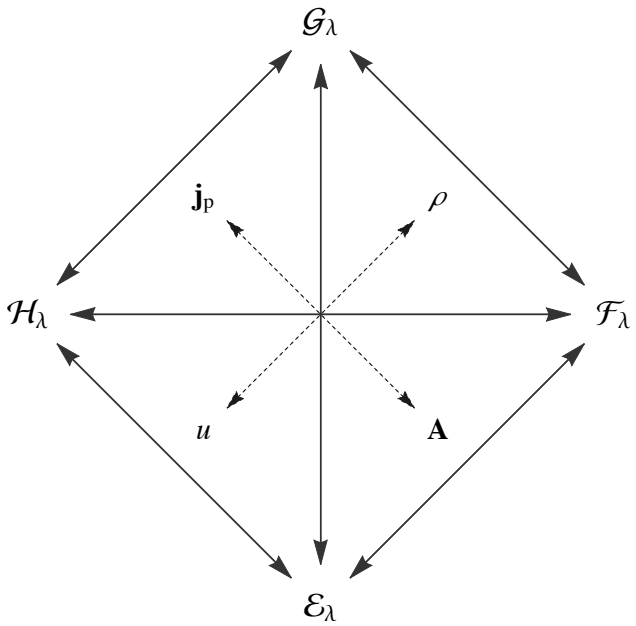

Figure 1: The four-way correspondence of DFT in a magnetic field, relating the concave function $\mathcal{E}_\lambda$, the concave–convex saddle function $\mathcal{F}_\lambda$, the convex function $\mathcal{G}_\lambda$, and the convex–concave saddle function $\mathcal{H}_\lambda$. Each function depends on the two adjacent variables. The downward conjugations $\rho \to u$ and $\mathbf{j}_\mathrm{p} \to \mathbf{A}$ are minimizations with positive pairings $+(u|\rho)$ and $+(\mathbf{A}|\mathbf{j}_\mathrm{p})$, respectively, while the upward conjugations $u \to \rho$ and $\mathbf{A} \to \mathbf{j}_\mathrm{p}$ are maximizations with negative pairings $-(u|\rho)$ and $-(\mathbf{A}|\mathbf{j}_\mathrm{p})$, respectively. The Hohenberg–Kohn variation principle corresponds in BDFT to the partial conjugation $\rho \to u$ from $\mathcal{F}_\lambda$ to $\mathcal{E}_\lambda$ in CDFT to the full conjugation $(\rho, \mathbf{j}_\mathrm{p}) \to (u, \mathbf{A})$ from $\mathcal{G}_\lambda$ to $\mathcal{E}_\lambda$.

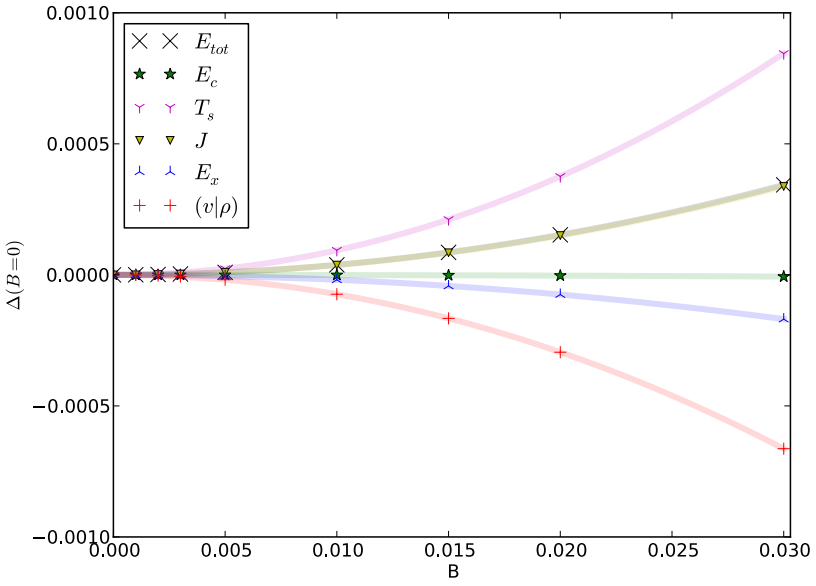

Figure 2: The Kohn–Sham energy components of H_2 relative to the zero-field values as a function of the magnetic field strength (atomic units, B in B_0 and Δ in E_h). The curves show the second-order approximation to the energy components (see text for details), with curvatures equal to the negative magnetizability at zero field (and its Kohn–Sham components). All calculations have been carried out at the FCI/aug-cc-pVTZ level of theory, at the zero-field equilibrium geometry.

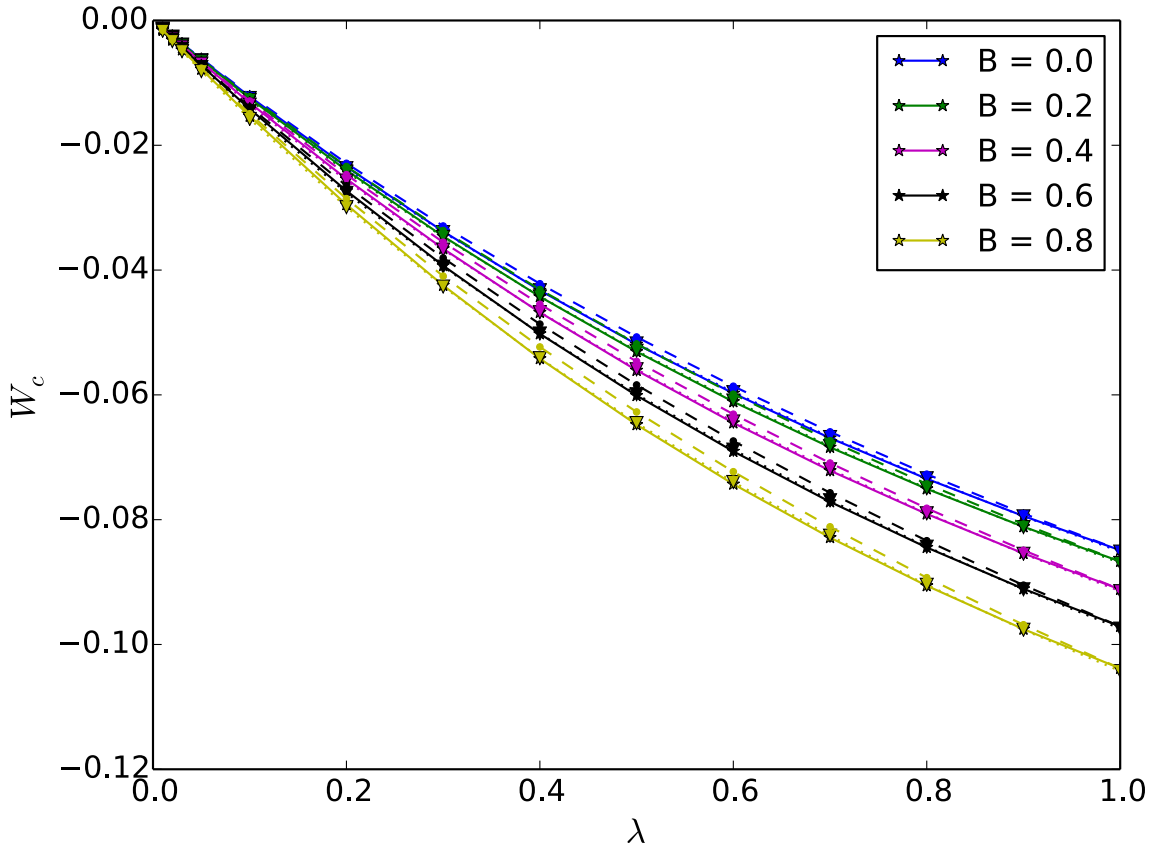

Figure 3: AC curves for H_2 at different magnetic field strengths with fixed bond length $2.1a_0$ (1.5 times the zero-field equilibrium bond length). The full lines show accurate *ab initio* AC integrands using the FCI density for each magnetic field strength. The dashed lines correspond to the THC model in Eq. (56) using $s = \mathcal{W}'(0)$ and $a = \mathcal{W}(1)$. The dotted lines show the same model with globally fitted parameters s and a, which are nearly on top of the accurate curves (atomic units, $\mathcal{W}_c$ in E_h).

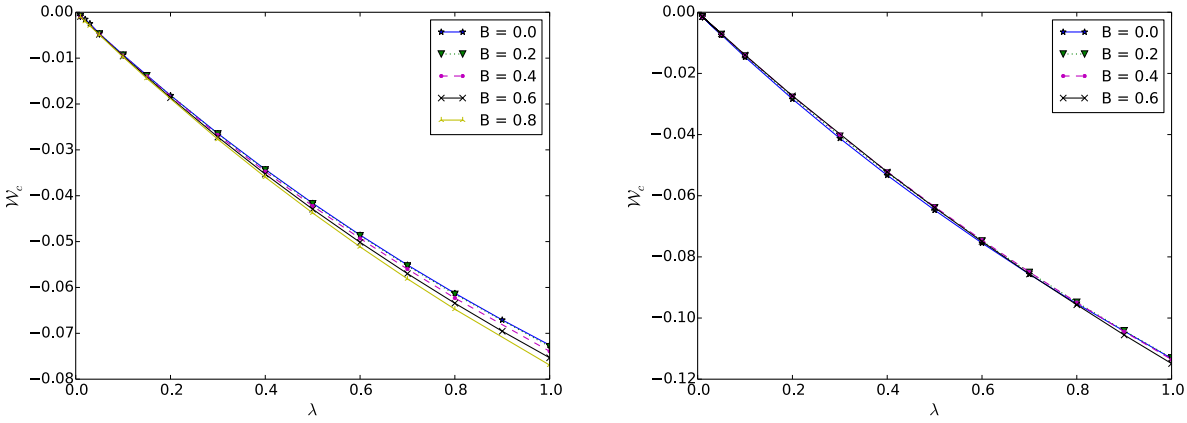

(a) H_2, calculations at the FCI / aug-cc-pVTZ level. (b) LiH, calculations at the CCD / aug-cc-pVTZ level.

Figure 4: AC curves of H_2 and LiH in a perpendicular magnetic field (atomic units, $\mathcal{W}_c$ in E_h). Each curve is calculated at the equilibrium bond distance in the applied field.

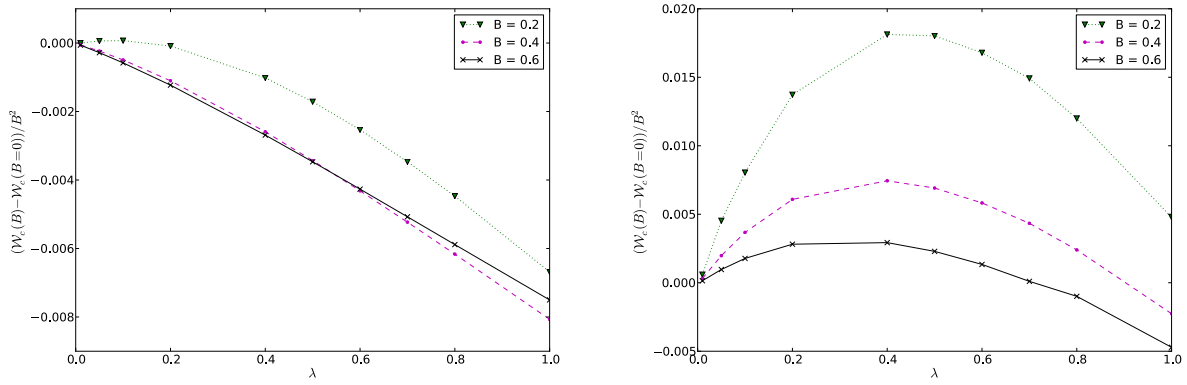

(a) H_2, calculations at the FCI / aug-cc-pVTZ level. (b) LiH, calculations at the CCD / aug-cc-pVTZ level.

Figure 5: $\Delta\mathcal{W}_c(B)$ curves of H_2 and LiH in a perpendicular magnetic field (atomic units, $\mathcal{W}_c$ in E_h). Each curve is calculated at the equilibrium bond distance in the applied field.

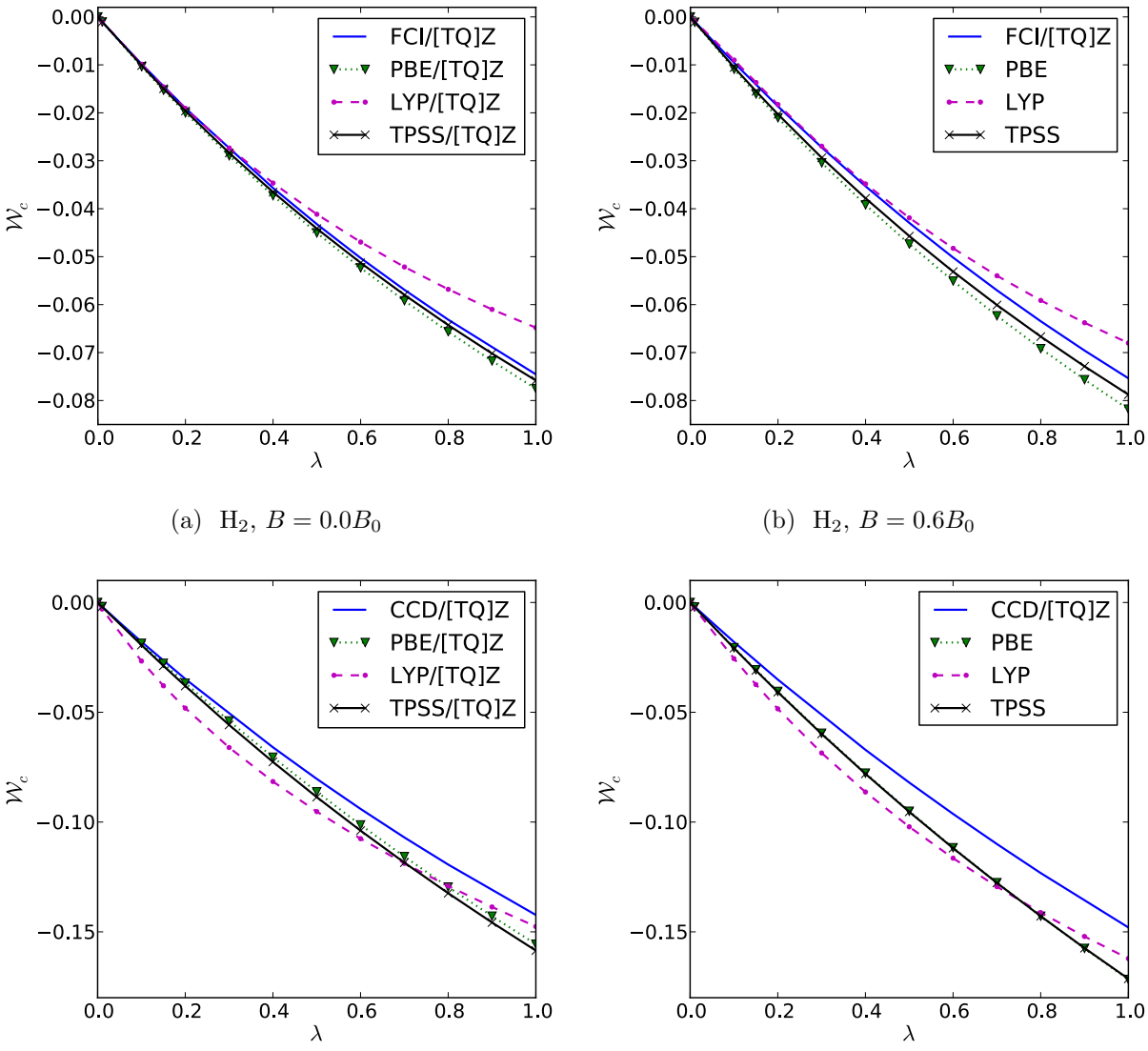

(a) H_2, $B = 0.0B_0$

(b) H_2, $B = 0.6B_0$

(c) LiH, $B = 0.0B_0$

(d) LiH, $B = 0.6B_0$

Figure 6: AC curves for H_2 and LiH with optimized density at each field strength (atomic units, $\mathcal{W}_c$ in E_h). For the DFA calculations the SCF density is used. For the *ab initio* calculations for H_2 the FCI density is used and for LiH the CCD density is used.